Title

Cancer recurrence monitoring using hyperpolarized [1-13C]pyruvate metabolic imaging in murine breast cancer model

Authors

Shin, Peter J
Zhu, Zihan
Camarda, Roman
et al.

Publication Date

2017-11-01

DOI

10.1016/j.mri.2017.07.014

Peer reviewed

HHS Public Access

Author manuscript

Magn Reson Imaging. Author manuscript; available in PMC 2018 November 01.

Published in final edited form as:

Magn Reson Imaging. 2017 November ; 43: 105–109. doi:10.1016/j.mri.2017.07.014.

Cancer Recurrence Monitoring using Hyperpolarized [1-^{13}C]Pyruvate Metabolic Imaging in Murine Breast Cancer Model

Peter J. Shin[1], **Zihan Zhu**[1,2], **Roman Camarda**[3], **Robert A. Bok**[1], **Alicia Y. Zhou**[4,5], **John Kurhanewicz**[1,2], **Andrei Goga**[3,4], and **Daniel B. Vigneron**[1,2]

[1]Department of Radiology and Biomedical Imaging, University of California at San Francisco, San Francisco, California, USA

[2]The UC Berkeley - UCSF Graduate Program in Bioengineering, California, USA

[3]Biomedical Sciences Graduate Program, University of California at San Francisco, San Francisco, California, USA

[4]Department of Cell and Tissue Biology, University of California at San Francisco, San Francisco, California, USA

Abstract

The purpose of this work was to study the anatomic and metabolic changes that occur with tumor progression, regression and recurrence in a switchable MYC-driven murine breast cancer model. Serial ^{1}H MRI and hyperpolarized [1-^{13}C]pyruvate metabolic imaging were used to investigate the changes in tumor volume and glycolytic metabolism over time during the multistage tumorigenesis. We show that acute de-induction of MYC expression in established tumors results in rapid tumor regression and significantly reduced glycolytic metabolism as measured by pyruvate-to-lactate conversion. Moreover, cancer recurrences occurring at the tumor sites independently of MYC expression were observed to accompany markedly increased lactate production.

Keywords

Cancer Recurrence; Breast Cancer; Hyperpolarized ^{13}C MRI; Metabolic Imaging

1. Introduction

One important factor that limits the success of cancer therapy in achieving complete cure or prolonged patient survivor is cancer recurrence. Although surgical removal and

Correspondence to: Peter J. Shin Byers Hall Room 102, 1700 4th st. University of California, San Francisco, San Francisco CA 94158, Tel: 1-415-514-4454, peter.shin@ucsf.edu.

[5]Current Address: Color Genomics, Burlingame, California, USA

chemotherapy can induce regression in primary tumors, such initial responses are commonly followed by relapsing malignancies, with the recurrent cancer often being much more aggressive than the original in terms of proliferative and metastatic capacities. Cancer relapse is thought to stem from multiple causes including primary tumors acquiring drug resistance (1,2), residual cancer cells surviving therapy (3), or the spreading of cancer cells to other parts of the body (metastasis) (4,5). Adjuvant systemic therapies are often done in clinics immediately following primary cancer treatments to prevent the cancer from coming back (6), yet a substantial number of patients remain at risk for late recurrences (7,8). Therefore, a non-invasive diagnostic tool that can detect local- or distant-site recurrences in their early stages is needed for improved individual patient management and to guide the development of novel therapeutics to counteract cancer relapse (9,10).

Cancer cells reprogram metabolic pathways in order to support their high rates of proliferation and growth (11,12). Such shifts in metabolism can be observed in all cancer types, and hence, is recognized as a hallmark of cancer (13). One particular example is the Warburg effect. It is the behavior of cancer cells to generate energy via a high rate of glycolysis followed by enhanced conversion of pyruvate to lactate, which is markedly different from the metabolism of normal non-proliferative cells. This altered metabolism in cancer can be monitored using recently developed hyperpolarized [1-^{13}C]pyruvate metabolic MRI methods. This molecular imaging approach uses dynamic nuclear polarization (DNP) to increase ^{13}C MRI signal more than a 10,000-fold (14), allowing the detection of enzymatic conversions of [1-^{13}C]pyruvate to its subsequent metabolites (15,16). The technique has been successfully applied to cancer imaging to assess tumor development (17-19), and response to therapies (20-22). The first hyperpolarized [1-^{13}C]pyruvate MRI study in prostate cancer patients demonstrated the potential and safety for future clinical studies (23).

In this study, we investigated the application of hyperpolarized [1-^{13}C]pyruvate metabolic imaging for the first time to monitor cancer recurrences in a switchable *c-MYC* mouse model of breast cancer. The goal was to test the hypothesis that glycolytic metabolism, as measured by pyruvate-to-lactate conversion, would decrease upon tumor regression initiated by switching off MYC expression in established tumors, but then would again increase even in relapsing tumors that are independent of MYC. We also experimented to detect the glycolytic change earlier in time before the recurring tumor showed morphologic changes.

2. Material and methods

2.1. Mouse Model of Breast Cancer

All animal studies were carried out under protocols approved by the local Institutional Animal Care and Use Committee (IACUC). We established a transgenic mouse line that conditionally expressed the human *c-MYC* oncogene in the mammary epithelium upon tetracycline administration as previously reported (24). Next, the animals were chronically treated with doxycycline for overexpression of the transgene until they developed mammary tumors. We surgically took out the tumor masses and kept them under cryopreservation to establish a bank of tumor grafts. Later, one of the tumor grafts was viably thawed, sectioned into small pieces, and serially transplanted to isogenic female FVB mice in the inguinal 4R

mammary gland, which phenocopied the original human *c-MYC* oncogene-induced tumor to a cohort of mice. Finally, the animals that bore the tumor grafts were treated with doxycycline immediately following the engraftments to induce tumor development from the onset.

2.2. Multistage Cancer Development

The tumor engrafted mice were kept under doxycycline treatment until their tumor growth reached approximately 2.5 centimeters in maximum diameter, at which time we performed baseline studies (see below for details) and withdrew doxycycline from the animals' diet for acute c-MYC deinduction. Following the withdrawal, all the animals exhibited rapid tumor regression within two weeks with the c-MYC-induced mammary tumors shrinking to visually unobservable states. Furthermore, after varying degrees of latency period, every animal exhibited tumor recurrences once again at the primary mammary sites without receiving any doxycycline treatment.

During the tumor progression, regression, and recurrence processes, we performed imaging studies on each animal on multiple dates. Each study included ^{1}H anatomical MRI scans for spatial referencing and tumor volume measurements, and hyperpolarized [1-^{13}C]pyruvate magnetic resonance spectroscopic imaging (MRSI) scans to monitor changes in glycolytic metabolism over time. After the last study, the animals were euthanized and the tumors were surgically resected.

2.3. Animal Experiment Setup

All imaging experiments were performed on a 3 T MRI scanner (GE Healthcare, WI, USA) equipped with 50 mT/m, 200 mT/m/ms gradients and a broadband RF amplifier. We used a custom built, ^{1}H/^{13}C dual-tuned mouse birdcage coil for RF transmit and signal receive (25). Prior to each experiment, animals were anesthetized with 2% isoflurane, and a catheter was inserted and secured into one of the tail veins of the animals to allow for intravenous (i.v.) injection of hyperpolarized media. The animals were placed inside the coil on top of a heating water pad and were kept under anesthesia during the experiments. We injected a 50 μL of diluted heparin-saline solution every 15 minutes to prevent the catheters from clogging.

2.4. ^{1}H MRI and ^{13}C MRSI

2D multislice anatomical images were acquired using a T_2-weighted fast spin echo (FSE) sequence. For each animal, 26 axial images were acquired in 256 × 256 grids with a field-of-view (FOV) of 4 cm, and 2 mm slice thickness. Additionally, 30 coronal images were acquired in 256 × 256 grids with a FOV of 8 cm, and 1 mm slice thickness. We used a HyperSense DNP system (Oxford Instruments, Abingdon, UK) operating at 3.35 T and 1.35° K to polarize samples consisting of 15 M [1-^{13}C]pyruvic acid in solution with 15 mM OX63 trityl radical and 0.5 mM of gadolinium. The hyperpolarized pyruvate samples were dissolved in a NaOH/TRIS buffer to a targeted pH value of 7.4 with 80 mM concentration. We injected 350 μL of this solution into the animals through the tail vein catheters over 12 seconds.

We acquired single time-point, ^{13}C MRSI data using a double spin-echo, symmetric echo-planar spectroscopic imaging (EPSI) sequence (26). 8 × 8 × 18 spatial points were encoded in the x, y, and z direction with 5 mm resolution for a voxel size of 0.125 cc. The EPSI gradient covered the data acquisition in the k_z-t dimension. The waveform had 102 msec duration with a spectral resolution of 9.8 Hz and a spectral bandwidth of 580 Hz. Also, TR was set to 215 msec and the flip angle was set to 10°. The ^{13}C 3D-MRSI scans started 30 seconds after the injection of hyperpolarized samples and lasted for 14 seconds.

2.5. Data Processing

We used OsiriX to manually draw region-of-interest (ROI) around tumors and to measure their volumes (27). We used the SIVIC open-source software package to process the ^{13}C MRSI data (28). Once the ^{13}C spectra were reconstructed, we integrated the area under each ^{13}C peaks to generate metabolic maps of lactate-to-pyruvate ratio. We then sinc-interpolated the maps, masked out all the background ^{13}C signals that were outside the imaging subject, and overlaid them on top of the proton anatomical images to visually display the measured metabolite distributions in vivo. Finally, we performed the paired ratio t-test for statistical inferences.

3. Results

3.1. Representative Data

A set of representative data that was acquired from an animal in the study is shown in Fig. 1. The animal developed a tumor in its inguinal 4R mammary gland while on doxycycline diet. At the baseline, the tumor volume was measured at 2.68 cm^3, which quickly regressed by approximately 50 percent to 1.24 cm^3 in four days once we took the animal off doxycycline treatment. A change in glycolytic metabolism in the tumor was also observed as measured by calculating lactate-to-pyruvate ratio (lac/pyr). For example, the lac/pyr values in tumor voxels (yellow box) changed drastically from 2.79 to 0.86 during the regression. The tumor further regressed to a visually unobservable size over time, and the animal remained in the regression state for a latency period. Finally, in seven weeks, as shown in the last column of Fig. 1, we observed a recurrent tumor (3.02 cm^3) forming once again at the primary site with elevated lactate production (lac/pyr = 2.44) measured in the tumor.

3.2. Monitoring of Multistage Cancer Development

All the animals in the study cohort indeed followed the same pattern of tumor progression, regression, and recurrence as shown in Fig. 2. More specifically, their tumors increased in size while doxycycline was administered, and quickly regressed within two weeks once doxycycline was removed. After the regression, all the animals stayed in dormant state for a latency period. Finally, relapses occurred at the mammary sites where the primary tumors were transplanted.

Changes in the glycolytic metabolism over time, as measured by hyperpolarized [1-^{13}C]pyruvate imaging, showed the similar trend as the volume changes. Lactate productions in the tumors were high when doxycycline was given and significantly decreased within two weeks once the animals were taken off doxycycline ($P < 0.001$).

Moreover, the tumor recurrences, which occurred without doxycycline administration, were accompanied by increased lactate production in the tumors ($P < 0.05$).

3.3. Early Detection of Cancer Recurrence

Given the above result, we performed a case study in which we sought to detect elevated lactate production earlier in time compared to tumor volume increase before the animal reached a full recurrence state. The result is shown in Fig. 3. Specifically, we made five measurements over time including a baseline study that was performed before putting the animal off doxycycline at day 0 (Fig. 3a). Tumor size and lac/pyr decreased until the sixteenth day at which point both the values reached their minimum of 0.54 cm^3 and 0.84, respectively (①). In the following days, we did not observe changes in the tumor volume by visual inspection. However, at the thirty-third day (②), we measured markedly increased lac/pyr value of 2.00 from the regressed tumor, whereas at this point the tumor volume only increased minimally to 0.75 cm^3. Finally, the animal reached its end-point at day 49 (③) with a fully established tumor volume of 3.02 cm^3 and further increased lac/pyr value of 2.64.

4. Discussion

In this study, we used a transgenic model of c-MYC-driven breast cancer in which transplanted tumor cells conditionally expressed the human *c-MYC* transgene only when doxycycline was given. This allowed us to switch on and off tumor growth in a controllable way by feeding the animals with and without doxycycline. We observed that ceasing *c-MYC* oncogene expression in established tumors results in rapid regression in terms of both tumor size and glycolytic metabolism. This data supports the previously described role of MYC in directly regulating glycolysis (12).

After being in the regression state for varying degrees of latency period, all the animals developed recurrent tumors at the location where the primary tumors had once developed. Surprisingly, the relapses occurred even though the animals were not fed with doxycycline. This suggests that a secondary driver that is independent of the transgenic *c-MYC* expression may be responsible for the tumor recurrences. Even in this case, we observed that high lactate production accompanied relapsing tumors. This is of clinical relevance since the detection of recurrence early and accurately by current imaging techniques remains a significant challenge. This study supports the potential use of hyperpolarized ^{13}C MR molecular imaging approach for “active surveillance” of cancer patients adding pyruvate-to-lactate conversion as a metabolic biomarker of recurrence. Identifying further biological causes of such recurrences and their role in affecting glycolytic metabolism could be another area of future study.

As shown in Figure 3, hyperpolarized [1-^{13}C]pyruvate imaging was able to detect increased lactate production earlier in time before the recurrent tumor showed eventual morphologic size changes. This observation supports the hypothesis that glycolytic alterations precede tumor formation in cancer relapses. The observation also suggests that hyperpolarized [1-^{13}C]pyruvate imaging combined with further preclinical and clinical patient studies (23) could be valuable in testing this hypothesis by identifying the temporal relationship between

oncogenic signaling, glycolytic pathway activity, and in vivo tumor formation in cancer relapses.

5. Conclusion

In this work, we applied hyperpolarized [1-^{13}C]pyruvate metabolic imaging to monitor metabolic changes that accompanied morphologic transformations in a multistage, murine breast cancer model. We further performed experiments that support the potential of hyperpolarized ^{13}C metabolic imaging to provide early diagnosis of recurrent cancers.

Acknowledgments

We thank Drs. Hsin-Yu Chen, Jeremy Gordon, and Peder Larson for their help in animal experiments. We also appreciate Drs. Ilwoo Park, Myriam Chaumeil, Celine Baligand, Renuka Sriram for their helpful discussions. This study was supported in part by National Institutes of Health (NIH) grants R01-CA170447, F99-CA212488-01, P41-EB013598, R01-CA183071, and CDMRP Era of Hope W81XWH-12-1-0272.

References

1. Holohan C, Van Schaeybroeck S, Longley DB, Johnston PG. Cancer drug resistance: an evolving paradigm. Nat Rev Cancer. 2013; 13:714–726. [PubMed: 24060863]
2. Kuczynski EA, Sargent DJ, Grothey A, Kerbel RS. Drug rechallenge and treatment beyond progression-implications for drug resistance. Nat Rev Clin Oncol. 2013; 10:571–587. [PubMed: 23999218]
3. Barker HE, Paget JTE, Khan AA, Harrington KJ. The tumour microenvironment after radiotherapy: mechanisms of resistance and recurrence. Nat Rev Cancer. 2015; 15:409–425. [PubMed: 26105538]
4. Gupta GP, Massagué J. Cancer metastasis: building a framework. Cell. 2006; 127:679–695. [PubMed: 17110329]
5. Weigelt B, Peterse JL, van't Veer LJ. Breast cancer metastasis: markers and models. Nat Rev Cancer. 2005; 5:591–602. [PubMed: 16056258]
6. Evans R, Tanguay J. Adjuvant therapy. Medicine. 2016; 44:39–41.
7. Brewster AM, Hortobagyi GN, Broglio KR, et al. Residual risk of breast cancerrecurrence 5 years after adjuvant therapy. J Natl Cancer Inst. 2008; 100:1179–1183. [PubMed: 18695137]
8. Heidenreich A, Bastian PJ, Bellmunt J, et al. EAU Guidelines on prostate cancer. Part II: Treatment of advanced, relapsing, and castration-resistant prostate cancer. Eur Urol. 2014; 65:467–479. [PubMed: 24321502]
9. Fidler IJ, Kripke ML. The challenge of targeting metastasis. Cancer and Metastasis Rev. 2015; 34:635–641. [PubMed: 26328524]
10. Li Y, Rogoff HA, Keates S, Gao Y, Murikipudi S, Mikule K, Leggett D, Li W, Pardee AB, Li CJ. Suppression of cancer relapse and metastasis by inhibiting cancerstemness. Proc Natl Acad Sci. 2015; 112:1839–1844. [PubMed: 25605917]
11. Hsu PP, Sabatini DM. Cancer Cell Metabolism: Warburg and Beyond. Cell. 2008; 134:703–707. [PubMed: 18775299]
12. Dang CV. Links between metabolism and cancer. Genes Dev. 2012; 26:877–890. [PubMed: 22549953]
13. Hanahan D, Weinberg RA. Hallmarks of Cancer: The Next Generation. Cell. 2011; 144:646–674. [PubMed: 21376230]
14. Ardenkjær-Larsen JH, Fridlund BR, Gram A, Hansson G, Hansson L, Lerche MH, Servin R, Thaning M, Golman K. Increase in signal-to-noise ratio of >10,000 times inliquid-state NMR. Proc Natl Acad Sci. 2003; 100:1–6. [PubMed: 12509507]
15. Brindle KM, Bohndiek SE, Gallagher FA, Kettunen MI. Tumor imaging usinghyperpolarized ^{13}C magnetic resonance spectroscopy. Magn Reson Med. 2011; 66:505–519. [PubMed: 21661043]

16. Kurhanewicz J, Vigneron DB, Brindle K, et al. Analysis of Cancer Metabolism by Imaging Hyperpolarized Nuclei: Prospects for Translation to Clinical Research. Neoplasia. 2011; 13:81–97. [PubMed: 21403835]
17. Chen AP, Albers MJ, Cunningham CH. Hyperpolarized C-13 spectroscopic imaging of the TRAMP mouse at 3T—Initial experience. Magn Reson Med. 2007; 58:1099–1106. [PubMed: 17969006]
18. Kettunen MI, Hu DE, Witney TH, McLaughlin R, Gallagher FA, Bohndiek SE, Day SE, Brindle KM. Magnetization transfer measurements of exchange between hyperpolarized [1-^{13}C]pyruvate and [1-^{13}C]lactate in a murine lymphoma. Magn Reson Med. 2010; 63:872–880. [PubMed: 20373388]
19. Hu S, Balakrishnan A, Bok RA, Anderton B, Larson PEZ, Nelson SJ, Kurhanewicz J, Vigneron DB, Goga A. ^{13}C-Pyruvate Imaging Reveals Alterations in Glycolysis that Precede c-Myc-Induced Tumor Formation and Regression. Cell Metab. 2011; 14:131–142. [PubMed: 21723511]
20. Day SE, Kettunen MI, Gallagher FA, Hu DE, Lerche M, Wolber J, Golman K, Ardenkjaer-Larsen JH, Brindle KM. Detecting tumor response to treatment using hyperpolarized ^{13}C magnetic resonance imaging and spectroscopy. Nat Med. 2007; 13:1382–1387. [PubMed: 17965722]
21. Park I, Mukherjee J, Ito M, Chaumeil MM, Jalbert LE, Gaensler K, Ronen SM, Nelson SJ, Pieper RO. Changes in pyruvate metabolism detected by magnetic resonance imaging are linked to DNA damage and serve as a sensor of Temozolomide response in glioblastoma cells. Cancer Res. 2014; 74:7115–7124. [PubMed: 25320009]
22. Asghar Butt S, Søgaard LV, Ardenkjær-Larsen JH, Lauritzen MH, Engelholm LH, Paulson OB, Mirza O, Holck S, Magnusson P, Åkeson P. Monitoring mammary tumor progression and effect of tamoxifen treatment in MMTV-PymT using MRI and magnetic resonance spectroscopy with hyperpolarized [1-^{13}C]pyruvate. Magn Reson Med. 2014; 73:51–58. [PubMed: 24435823]
23. Nelson SJ, Kurhanewicz J, Vigneron DB, et al. Metabolic Imaging of Patients with Prostate Cancer Using Hyperpolarized [1-^{13}C]Pyruvate. Sci Transl Med. 2013; 198:1–11.
24. D'Cruz CM, Gunther EJ, Boxer RB, et al. c-MYC induces mammary tumorigenesis by means of a preferred pathway involving spontaneous. Nat Med. 2001; 7:235–239. [PubMed: 11175856]
25. Derby K, Tropp J, Hawryszko C. Design and evaluation of a novel dual-tuned resonator for spectroscopic imaging. J Magn Reson. 1990; 86:645–651.
26. Larson PEZ, Kerr AB, Swisher CL, Pauly JM, Vigneron DB. A rapid method for direct detection of metabolic conversion and magnetization exchange with application to hyperpolarized substrates. J Magn Reson. 2012; 225:71–80. [PubMed: 23143011]
27. Rosset A, Spadola L, Ratib O. OsiriX: An Open-Source Software for Navigating in Multidimensional DICOM Images - Springer. Journal of digital imaging. 2004
28. Crane JC, Olson MP, Nelson SJ. SIVIC: Open-Source, Standards-Based Software for DICOM MR Spectroscopy Workflows. Int J of Biomedical Imaging. 2013:1286–1289.

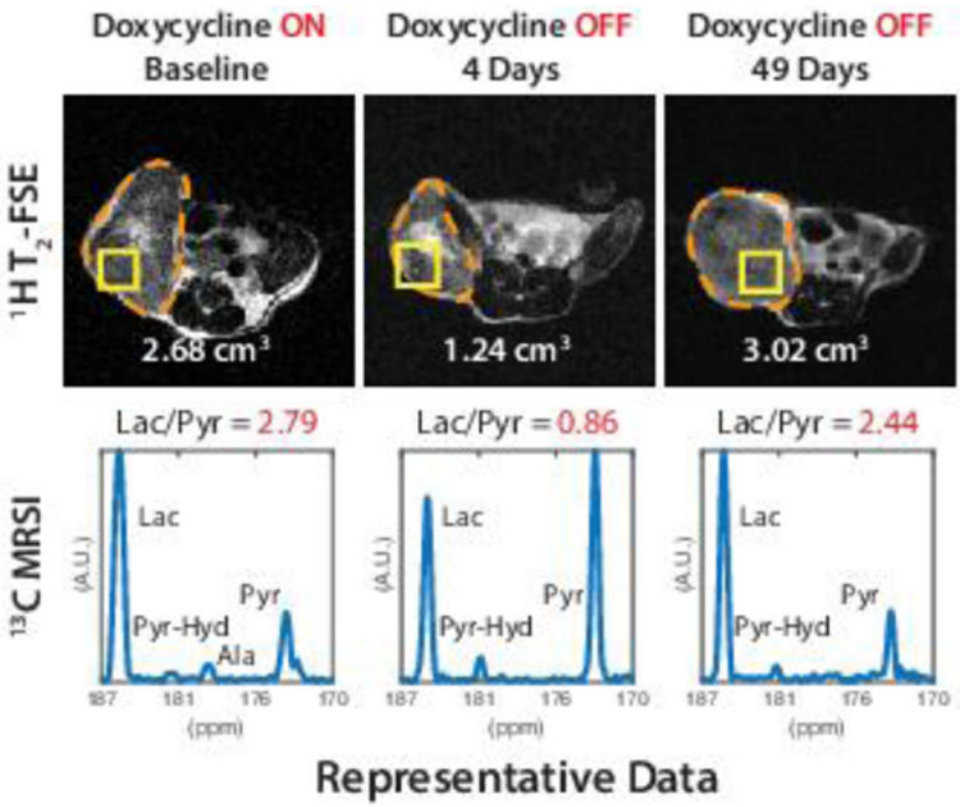

Figure 1.

Representative ^{1}H anatomical axial images (top row) and hyperpolarized ^{13}C spectra (bottom row) showing changes in tumor volume and glycolytic metabolism over time. Tumors are outlined in dashed lines with their measured volume values annotated in the anatomical images. Voxel locations that correspond to the ^{13}C spectra are marked with square boxes. The voxel size was 0.125 cc. The spectra are shown in arbitrary units (A.U.). The peaks are labeled as Lac (lactate), Pyr (pyruvate), Ala (alanine), and Pyr-Hyd (pyruvate hydrate). At the baseline (first column), the animal had a large tumor that showed high lactate-to-pyruvate ratio (lac/pyr). Four days after taking the animal off doxycycline, the tumor regressed by 50% and lower lac/pyr values were measured (middle column). Finally, after a latency period, the tumor reoccurred at the primary site showing high lac/pyr in the recurrent tumor (last column).

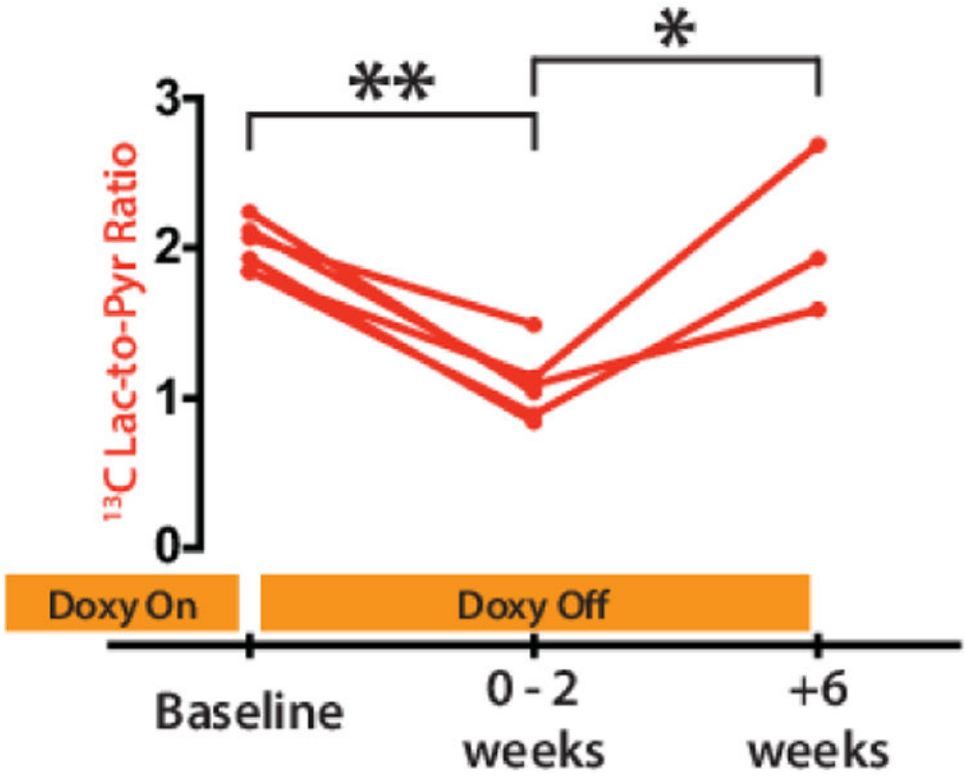

Figure 2.

Changes in glycolytic metabolism in multistage cancer development. Red lines represent the changes in lactate-to-pyruvate ratio (lac/pyr) over time. Tumors showed decreased glycolytic activity when the animals were taken off doxycycline (**, $P < 0.001$). However, tumors recurred in a doxycycline independent manner and elevated lac/pyr values were observed in the recurrent tumors (*, $P < 0.05$).

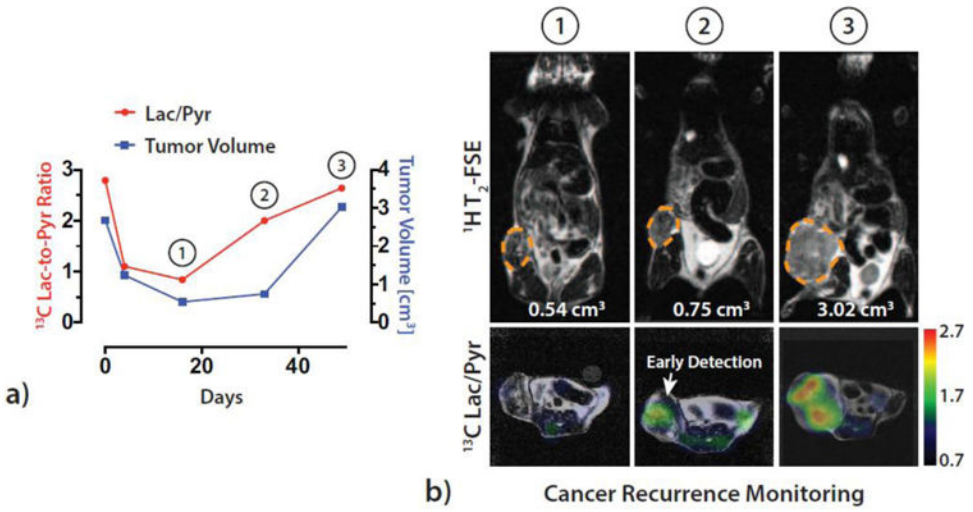

Figure 3.

Early detection of cancer recurrence with hyperpolarized [1-^{13}C] pyruvate metabolic imaging. a) Graphs of changes in ^{13}C lactate-to-pyruvate ratio (lac/pyr, red line) and tumor volume (blue line) over time. We used the maximum lac/pyr values measured within the tumor voxels. The baseline study was performed at day zero and four follow-up measurements were made. b) ^{1}H anatomical images (coronal, top row) and hyperpolarized ^{13}C lac/pyr maps (bottom row) measured at three different time points: 16 days, 33 days, and 49 days. Tumors are outlined in dashed lines with their measured volumes annotated in the anatomical images. Note that the increase in lactate production was detected earlier in time than the increase in volume in the recurrent tumor.